A Connectome-Based Approach to Assess Motor Outcome after Neonatal Arterial Ischemic Stroke

Mariam Al Harrach[a,b], Pablo Pretzel[c], Samuel Groeschel[c], François Rousseau[d], Thijs Dhollander[e], Lucie Hertz-Pannier[f], Julien Lefevre[g], Stéphane Chabrier[h,i], Mickael Dinomais[a,j], on behalf of the AVCnn study group

a Université d'Angers, Laboratoire Angevin de Recherche en Ingénierie des Systèmes (LARIS) EA7315, 49000 Angers, France
b Université de Rennes 1, Laboratoire Traitement du Signal et de l'Image (LTSI), INSERM U1099, F-35000 Rennes, France
c Experimental Paediatric Neuroimaging, Department of Child Neurology, University Hospital Tübingen, Germany
d IMT Atlantique, INSERM U1101 LaTIM, UBL, 29200 Brest, France
e Developmental Imaging, Murdoch Children's Research Institute, Melbourne, Australia
f UNIACT, Neurospin, Institut Joliot,CEA-Paris Saclay, and Inserm U114;Universite de Paris, Gif sur Yvette, F-91191, France
g Institut de Neurosciences de la Timone UMR 7289, Aix Marseille Université, CNRS, 13385 Marseille, France.
h INSERM, UMR1059 Sainbiose, Univ Saint-Etienne, Univ Lyon, F-42023 Saint-Etienne, France
i CHU Saint-Etienne, French Centre for Paediatric Stroke, Paediatric Physical and Rehabilitation Medicine Department, INSERM, CIC 1408, F-42055 Saint-Etienne, France
j CHU Angers, Departement de Medecine Physique et de Readaptions and LUNAM, Angers, France.

* See Appendix S1 (online supporting information) for full list of members.

Correspondance to : Mariam Al Harrach

Laboratoire de Traitement du Signal et de l'Image (LTSI)

Equipe Sesame (Systemes Epileptogenes : signaux et modèles)

Université de Rennes 1, Campus de Beaulieu, bat 22
Email : mariam.alharrach@univ-rennes1.fr

Abstract

Studies of motor outcome after Neonatal Arterial Ischemic Stroke (NAIS) often rely on lesion mapping using MRI. However, clinical measurements indicate that motor deficit can be different than what would solely be anticipated by the lesion extent and location. Because, this may be explained by the cortical disconnections between motor areas due to necrosis following the stroke, the investigation of motor network can help in the understanding of this discrepancy between visual inspection and outcome. In this study, we propose to examine the structural connectivity between motor areas in NAIS patients in comparison to healthy controls in order to define the cortical and subcortical connections that are can depict motor outcome. Accordingly, 30 healthy controls and 32 NAIS patients with and without Cerebral Palsy (CP) underwent MRI acquisition and manual assessment. The connectome of all participants was obtained from T1-weigted and diffusion weighted imaging. Results showed significant disconnections in the lesioned as well as the contra-lesioned hemisphere of patients. Furthermore, significant correlations were found between the structural connectivity metric of specific motor areas and manuality assessed by the Box and Block Test (BBT) scores in patients. Using the connectivity measures of these links we were able to estimate the BBT score using a multiple linear regression model. Based on one connection value we were also able to predict the presence or not of CP. According to our results, structural connectome, can be an asset in the estimation of gross manual dexterity after neonatal stroke.

Keywords: Neonatal arterial ischemic stroke, structural connectivity, connectome, box and block test, cerebral palsy, diffusion weighted imaging, MRI.

Abbreviations: NAIS = Neonatal Arterial Ischemic Stroke, Box and Block Test, LH= Left Hemisphere, RH= Right Hemisphere, CP=Cerebral Palsy.

1. Introduction

Neonatal Arterial Ischemic Stroke (NAIS), affecting 1 in 3200 births, is defined as a cerebrovascular accident taking place between birth and 28 days of life with clinical or radiological evidence of focal arterial infarction (Dunbar and Kirton, 2018; Fluss et al., 2019; Raju et al., 2007). It is recognised as a major cause of early brain injury and lasting disability (Dunbar and Kirton, 2018; Fluss et al., 2019) and is found to be the prominent cause of unilateral cerebral palsy (CP) in term-born children (Kirton and deVeber, 2015). Moreover, studies demonstrated that at least two-third of patients will exhibit some neurodevelopment disabilities at school-age (Chabrier et al., 2016; Kirton Adam and deVeber Gabrielle, 2013).

Many studies attempted to identify the predictors of motor impairment in stroke using various neurological and imaging methods that ranged from lesion localization and characterisation (voxel-wise lesion symptom mapping (VLSM)) to motor system analysis using functional and structural data collected from MRI, fMRI and Diffusion Tensor Imaging (DTI) techniques (Husson et al , 2010: Chabrier et al., 2016; Dinomais et al., 2015a; Jang, 2010; Song et al., 2015). Recent studies proposed new biomarkers for motor outcome following stroke. These biomarkers included corticospinal tract (CST) lesion measures such as the study of Feng et al. that proposed a weighted CST lesion load depicting the weight of the lesion on the CST tract . However, this study only focused on the outcome at 3 months post stroke. Another work proposed by Yoo et al. attempted to predict patients hand function following stroke by inspecting the fiber number and fractional anisotropy in different parts of the CST (Yoo et al., 2019). Although they reported that CST integrity was related to the hand function, their study was limited due to the lack of quantitative tools for the assessment of hand function. Some studies attempted to analyse the stroke motor outcome by inspecting both structural and functional

integrity measures of the motor systems (Lam et al., 2018). They found that each of these biomarkers provide a distinct information about outcome. Nevertheless, Lin et al. demonstrated that functional connectivity measures were weaker than CST integrity-based ones in the prediction of motor recovery (Lin et al., 2018).

During the last decade, structural connectomics studies have proven to be valuable in understanding brain structure (Taylor et al., 2017), disorders (Taylor et al., 2018) and development (Lim et al., 2015). In particular, cortical disconnections of specific areas were found to be related to clinical deficits (Bonilha Leonardo et al., 2014; Yourganov et al., 2016). These studies demonstrated that connectome-based analysis can establish a relation between cortical areas connections and a clinical outcome (score) (Bonilha Leonardo et al., 2014; Yourganov et al., 2016). Despite this, there is still a lack of structural connectivity-based studies of motor functions in childhood stroke and even more in NAIS.

For this purpose, we aimed to investigate the structural connectivity of the motor system's cortical and subcortical regions following NAIS in comparison to healthy controls in order to determine the cortical connections that describes the motor outcome at 7 years. The motor outcome was delineated by the Box and Block Test (BBT) score as well as the presence of CP. The connections were then used as inputs in the estimation process. We used both multiple linear regression and artificial intelligence techniques for the prediction of motor outcome prognosis. The patients were also divided into two groups based on the side of their lesion (left or right hemisphere) in order to study the impact of stroke laterality on the motor outcome.

2. Materials and methods

2.1. Subjects

The participants in this study belonged to a cross-sectional analysis at age 7 years of the AVCnn database (Accident Vasculaire Cérébral du nouveau-né, that is, neonatal stroke; PHRC régional n°03-08052 and PHRC interrégional n°10-08026; Eudract number 2010-A00329-30). This cohort was described in detail elsewhere (Chabrier et al., 2016; Dinomais et al., 2015a). In a few words, 100 term newborns with an arterial cerebral infarct, confirmed by early brain imaging (CT and/or MRI before 28 days of life), who were symptomatic during the neonatal period (thus matching the 2007 definition of NAIS (Chabrier et al., 2016)) were consecutively enrolled between November 2003 and October 2006 from 39 French centers. 72 children took part in a clinical, neuropsychological and language assessment at 7 years ($AVCnn^{7ans}$). During this assessment an MRI was proposed to the families. 52 children participated in this MRI study ($AVCnn^{signal}$; PHRC 2010-07; Eudract number 2010-A00976-33). Among them, 38 had a unilateral lesion in the median cerebral arterial (MCA) territory. However, after further examination six patients were excluded due to poor segmentation results (for more details please refer to (Dinomais et al., 2015a)), leaving 32 patients. They constituted the patient population of this study.

Based on a previous study that indicates different outcomes following the side of the lesion (Harrach et al., 2019), Patients were divided into two groups: patients with lesion in the left hemisphere (LLP) and patients with lesions in the right hemisphere (RLP). In addition to the LLP and RLP patients we recruited 30 healthy controls (HC). These controls were matched in age and gender with the patients (Dinomais et al., 2015a). General characteristics of the participants are presented in Table 1 and a detailed description of the patients is presented in Supplementary Table A.

Informed written consent respecting the declaration of Helsinki was obtained from all participants/parents as well as approval from the ethical committee of the university hospital of

Angers, France. Handedness was determined according to the Edinburgh inventory (Oldfield, 1971).

Table 1: General profile of the participants.

	HC	LLP	RLP	
	Mean (±std) or n (%)	**Mean (±std) or n (%)**	**Mean (±std) or n (%)**	**p-value***
Number (n)	30	18	14	---
Age (years)	7.71 (±0.54)	7.23 (± 0.13)	7.28 (±0.20)	0.543
Gender	Males: 14 (47%) Females: 16 (53%)	Males: 10 (56%) Females: 8 (44%)	Males: 9 (64%) Females: 5 (36%)	0.376[a]
Right-handed	27 (90 %)	6 (33 %)	14 (100 %)	0.180[a]
Lesion size (ml)	____	32.45 (± 33.21)	38.16 (± 46.94)	0.859
TIV	1395.4 (± 110.01)	1307.0 (± 157.71)	1277.7 (± 98.30)	0.127

HC: Healthy Controls, **LLP:** Left Lesioned Patients, **RLP:** Right Lesioned Patients,

TIV: Total intracranial volume

* p-values are obtained by one-way Kruskal Wallis non-parametric ANOVA

[a] Chi squared test

2.2. Manual dexterity of contra- and ipsilesional hands

The motor performance of the ipsi- and contralesional hands of all NAIS patients were assessed using the Box and Block Tests (BBT). The BBT is an approved tool for measuring gross manual dexterity in children (Mathiowetz et al., 1985). It consists of a box with two compartments separated in the middle. At the beginning, 100 small blocks are located in one of the compartments, on the same side of the tested hand. Children move as many cubes as they can from one compartment to the other. Both hands were evaluated. The individual score was

obtained by counting the maximum number of cubes transferred by the ipsi- and contralesional hand in 1 min, thus the higher, the better.

2.3 Cerebral palsy

The evaluation team included either a pediatric neurologist or a pediatric physical and rehabilitation medicine practitioner experienced in children disability. The definition given by the Surveillance for CP in Europe was used: permanent abnormal tone or decreased strength as a consequence of a non-progressive early brain injury (present by definition in our population), and associated with a patent functional deficit (Cans et al., 2007).

2.3. *MRI acquisition and processing*

2.3.1. Acquisition

Images were acquired on a 3.0 Tesla scanner (MAGNETOM Trio Tim system, Siemens, Erlangen, Germany, 12 channel head coil) at Neurospin, CEA-Saclay, France. Two Imaging sequences were collected for each participant.

The first was a high-resolution 3D T1- weighted volume using a magnetization-prepared rapid acquisition gradient-echo sequence [176 slices, repetition time (TR) 2300 msec, echo time (TE) 4.18 msec, field of view (FOV) 256 mm, flip angle=9°, voxel size $1 \times 1 \times 1$ mm^3].

The second was a diffusion-weighted dual SE-EPI sequence with 30 diffusion encoding directions and a diffusion-weighting of b=1,000 s/mm2 (TR= 9,500 msec, TE= 86 msec, 40 slices, voxel size $1.875 \times 1.875 \times 3$ mm^3).

2.3.3. Lesion Masks

For each patient, the boundaries of the lesion were manually delineated on a slice by slice basis by two of the authors (MD, SG) that were blinded to the clinical information, especially motor function. This delineation was performed on the individual 3D T1 images to create a binary lesion mask using the MRIcron software (http:// www.mccauslandcenter.sc.edu/mricro) (Rorden et al., 2007). In case of a main branch MCA stroke, the lateral border of the lesion mask was drawn along the inner border of the skull, comprising the whole porencephaly (Dinomais et al., 2015b).

2.3.4. DWI preprocessing and fiber tracking

The diffusion images were processed using MRtrix3 software (https://www.mrtrix3.com) running on Ubuntu 18.04.2 LTS machine. Preprocessing of DWI images included denoising (Veraart et al., 2016b, 2016a), unringing to remove Gibb's artefacts (Kellner et al., 2016), motion and distortion correction (Andersson and Sotiropoulos, 2016). Fiber Orientation Distribution (FOD) was obtained using constrained spherical deconvolution (CSD) (Tournier et al., 2007, 2004). The FODs were then corrected for the effects of residual intensity inhomogeneities using multi-tissue informed log-domain intensity normalization (Raffelt et al., 2017). In order to create the whole brain tractogram, a probabilistic algorithm that performs a second-order Integration over FOD was used (Tournier et al., 2009). The maximum angle between successive steps was set to 60 degrees and the cutoff value was fixed at 0.2. One million streamlines tractogram was obtained per subject. Finally, these streamlines were filtered into 200000 streamlines using Spherical-deconvolution Informed Filtering of Tractograms (SIFT) to reduce CSD-based bias in overestimation of longer tracks compared to shorter tracks (Smith et al., 2013). The subject specific proportionality coefficient μ defined by the SIFT model was

computed for the inter subject comparison which will be discussed further-on in this section. All the aforementioned steps were performed in the diffusion native space.

2.3.5. Brain parcellation

The first step of brain parcellation consisted of preprocessing of the T1 weighted images of all the subjects using the FreeSurfer suite, version 6.0.0 (https://surfer.nmr.mgh.harvard.edu/), on a single DELL workstation running ubuntu 16.04 LTS (Intel R Core TM i7-7820HQ CPU @ 2.9GHz × 8). Preprocessing steps included classification of the grey and white matters as well as segmentation of subcortical structures.

The atlas used for the Structural Connectivity (SC) analysis was that of Glasser et al. (Glasser et al., 2016). This atlas divides the cortical gray matter into 180 atlas regions per hemisphere. Subsequently, using Freesurfer, we constructed the volumetric atlas-based parcellation images for each subject including the 180 × 2 grey matter regions as well as 19 subcortical regions based on the FreeSurfer segmentation (9 × 2 homologs consisting of cerebellum, thalamus, caudate, putamen, pallidum, hippocampus, amygdala, accumbens and ventral Dorsal Caudate (DC) plus brainstem). Accordingly, the obtained parcellation image included 379 distinct atlas regions in total.

For the NAIS patients, explicit lesion masking was performed before the parcellation to minimize the impact of the lesion on the estimates (Gleichgerrcht et al., 2017).

In order to compute the structural connectivity matrix, we registered the volumetric atlas-based parcellation images into the individual diffusion space of the corresponding subject using the FSL FLIRT suite (FMRIB's Linear Image Registration Tool, https://fsl.fmrib.ox.ac.uk/fsl/fslwiki/FLIRT). Then, using MRtrix, the atlas-based parcellation in diffusion space was overlayed onto the whole brain tractogram which allowed us to identify the set of fibers F(i , j) connecting each pair of nodes representing the atlas regions i and j. The metric was collect-

ed in a 379 × 379 matrix defined as the connectivity matrix where each cell c(i, j) represents the number of streamlines connecting the areas i and j. The diagonal of the connectivity matrix was set to zero in order to discard the connections in the same atlas area.

However, we have to point out that this metric is highly dependent on the atlas region volume as well as the overall intracranial volume. Accordingly, for group comparisons these matrices were normalized by the individual brain volume (Xie and He, 2012; Yourganov et al., 2016) and multiplied by the proportionality coefficient previously mentioned (Smith et al. 2013).

The block diagram presenting an overview of the methodology used in order to obtain the structural connectivity matrix is depicted in Figure 1.

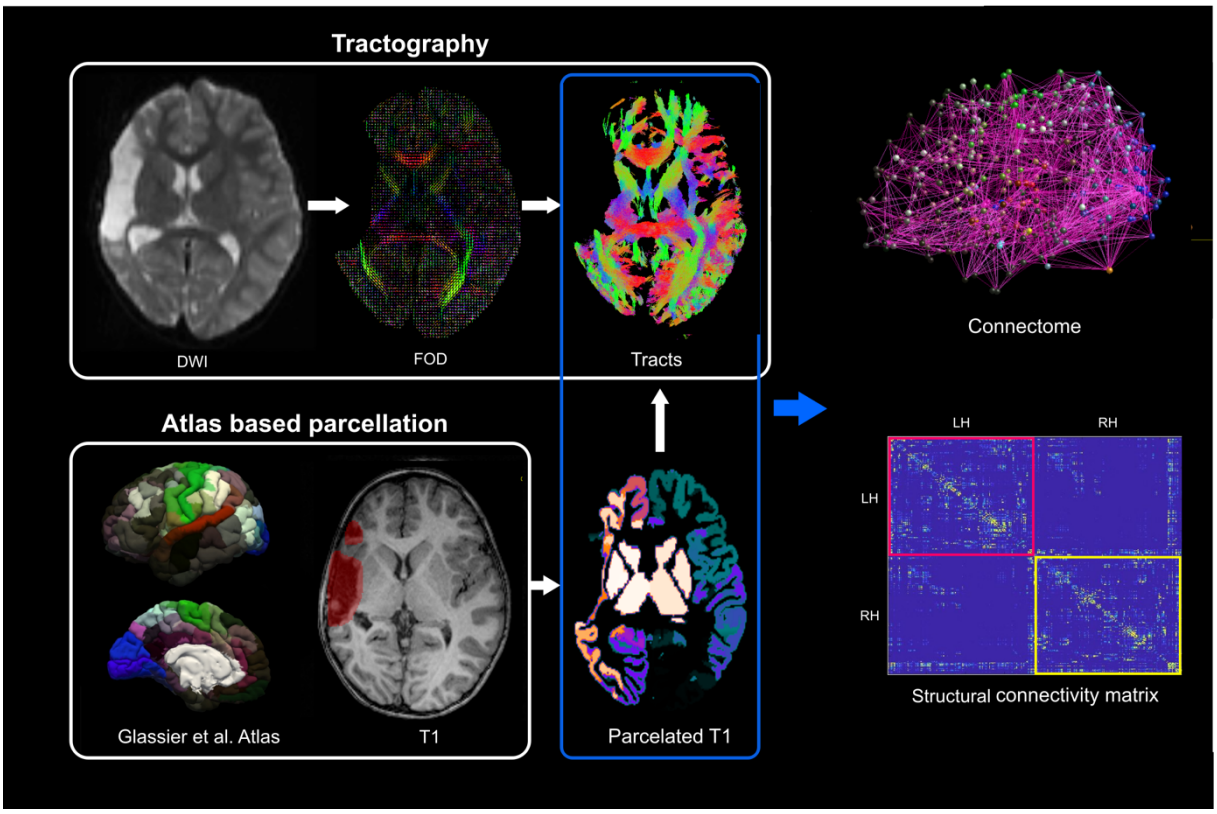

Figure 1: Overview of the methodology. The creation of the structural connectivity matrix consists of different steps. These steps include the processing of T1 weighted images (second row) with FreeSurfer and FSL as well as diffusion weighted images with MRtrix3 (first row). The obtained connectivity matrix consists of 379 × 379 connections weights.

2.3.6 Motor connectivity mapping

In this work we were interested in the impact of the NAIS on the motor outcome in particular. The cerebral areas responsible for motor performance and dexterity constituted the so-called brain motor system (Bioulac et al., 2004; Glasser et al., 2016; Rowe and Siebner, 2012) and are presented in Table 2. Consequently, the 52 × 52 motor connectivity matrix, that reflects the connections between the motor areas, was extracted from the 379 × 379 structural connectivity matrix as depicted in Figure 2.A. Afterwards, in order to reduce the number of connections to analyse, to connections of interest, we computed the mean motor connectivity matrix of the control group and then we only kept the cells that were higher than 10% of the maximum connection value (Figure 2.B). In this manner, we only kept the main links that describe the connections between the motor areas. These links are divided into intra- (LH ⇔ LH and RH ⇔ RH) and inter-hemisphere (LH ⇔ RH) connections and are presented in Table 3 and Figure 2.C.

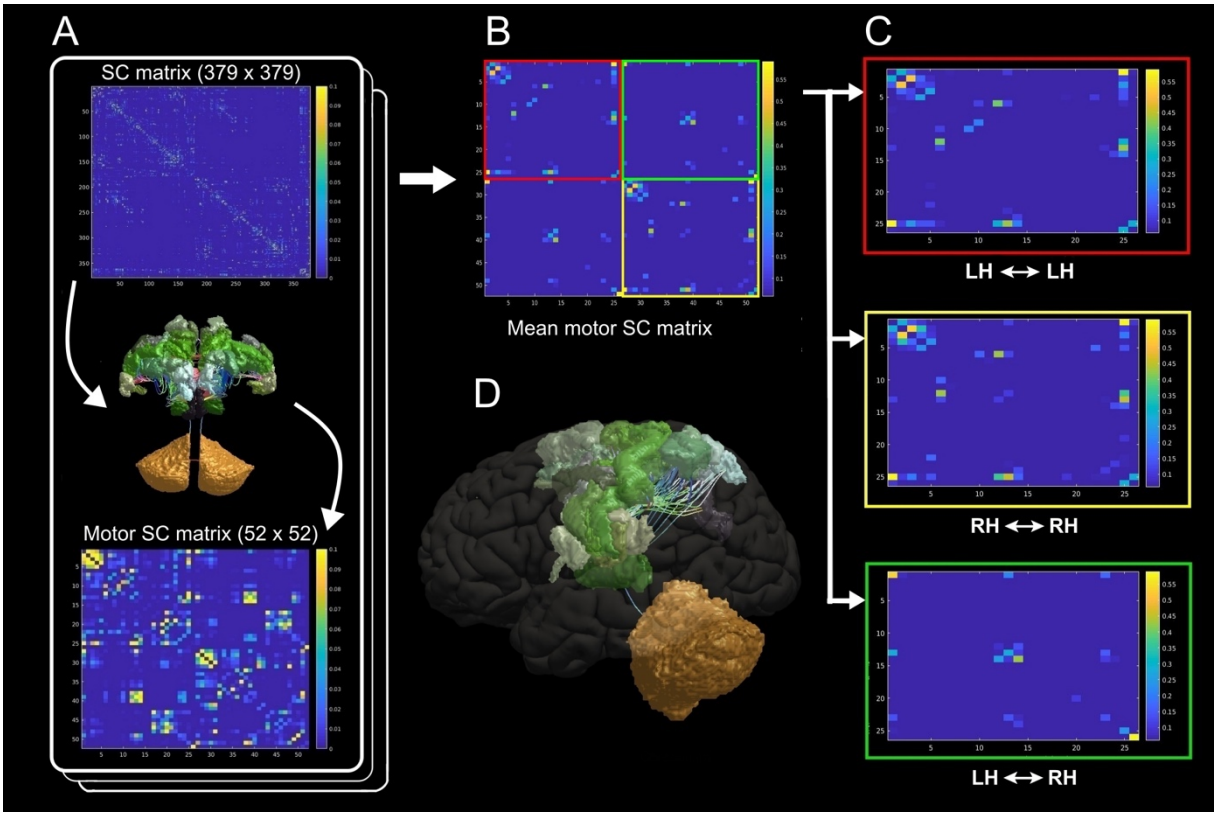

Figure 2: General process of connection selection. A. Extracting the motor SC matrix from the whole brain 379 × 379 matrix. With 24 motor areas in each hemisphere 52 nodes were obtained. B. The mean motor SC for the control group. C. The connections of interest chosen for this study. D. Illustration of the motor connectome for the left hemisphere.

2.4. Statistical Analysis

Statistical tests across groups were conducted using Matlab 2017a. For the comparison between healthy and patient groups, Two-sample Kolmogorov-Smirnov test was used since the samples did not follow a normal distribution. We used Pearson's correlation coefficient to measure the linear correlation between the connectivity metric and the corresponding BBT score as well as the presence or not of CP. All results with $p < 0.05$ were considered significant.

2.5. Estimation of motor outcome

MLR

To model the relationship between the brain connections of interest in the motor area and the motor performance, we used a multiple linear regression model (MLR). This model is used to estimate the BBT score of the contralesional (affected) hand from a group of structural connection scores chosen as links of interest (LOI)s. These LOIs were determined after a correlation analysis between the BBT scores and the motor SC scores or connectivity metrics. The estimated MLR model can be presented by the following equation:

$$y = w_0 + w_1 x_1 + w_2 x_2 + \cdots + w_n x_n + \varepsilon$$

Where y is the BBT score, x_i is the connection score of the ith connection of interest (the links that are significantly correlated with the BBT score), w_i is the slope coefficient of each x_i, ε is the constant offset term and n is the number of features (correlated links scores).

The accuracy of the estimation was computed following the leave-one-participant-out cross validation technique. Accordingly, one patient was excluded, and the remaining patients were used for the training of the MLR model. Afterwards, the model was evaluated by estimating the BBT score of the excluded patient using the model. This process was repeated so each time a different patient was excluded until all patients had a turn. The accuracy is then evaluated by computing the estimation error percentage between the real and estimated values of BBT.

KNN

To predict the presence or not of CP, a K Nearest Neighbor KNN classification model was used. For each group of patients (LLP and RLP), motor connectivity values were used as features in order to train the KNN model. The accuracy of the prediction was evaluated using

also the leave-one-participant-out cross validation technique. The accuracy was then computed as the percentage of correctly classified patients (that were not a part of the training set) between CP or no CP.

Table 2: The motor cortical areas and corresponding sub-areas used for the motor connectivity mapping. The Abbreviations used are the same as in (Glasser et al., 2016).

Motor areas and sub-areas	
Primary motor cortex (M1)	**Cingulate cortex (CC)**
	Dorsal part of 24d (24dd) Ventral part of 24d (24dv)
Primary somatosensory cortex (S1)	**Parietal cortex (PC)**
BA3a Fundus of the central sulcus BA3b posterior bank of the sulcus BA1 BA2	Medial Area 7P (7 Pm) Medial BA 7 (7m) Lateral area 7A (7AL) Medial Area of 7A (7Am) Lateral part of Area 7P (7 PL) 7 PC
Secondary somatosensory cortex (S2)	**Supplementary (SMA)**
Posterior part of Brodmann's 43 (OP4) Frontal OPercular area (PFOP)	Lateral BA6 (6ma) Posterior BA6 (6mp) Supplementary and cingulate eye fields (SCEF)
Premotor cortex (PMC)	**Thalamus**
Anterior part of BA6 (6a) ventral part of BA6(6v) Rostral part of BA6 (6r) Area bounded by FEF and PEF (55b) Frontal Eye Field (FEF) PreFrontal Eye Field (PEF)	**Cerebellum**

*BA: Brodmann Area

Table 3: The intra- and inter-hemisphere links used in the motor function connectivity analysis.

Intra-hemisphere connections used in connectome-based analysis			
1	M1 ←→ BA 3a	**18**	BA2 ←→ 7PC
2	M1 ←→ BA 3b	**19**	BA2 ←→ thalamus
3	M1 ←→ BA 1	**20**	6a ←→FEF
4	M1 ←→ 6V	**21**	6a ←→6ma
5	M1 ←→ 6mp	**22**	6a ←→ 6mp

6	M1 ←→ thalamus	**23**	6a ←→ thalamus
7	M1 ←→ cerebellum	**24**	55b ←→ FEF
8	BA3a ←→ BA3b	**25**	6ma ←→ 6mp
9	BA3a ←→ BA1	**26**	6ma ←→ thalamus
10	BA3a ←→ BA2	**27**	6mp ←→ 24dd
11	BA3a ←→ thalamus	**28**	6mp ←→ thalamus
12	BA3b ←→ BA1	**29**	SCEF ←→ 24 dv
13	BA3b ←→ BA2	**30**	SCEF ←→ thalamus
14	BA3b ←→ thalamus	**31**	7AL ←→ thalamus
15	BA1 ←→ BA2	**32**	24dd ←→ thalamus
16	BA1 ←→ thalamus	**33**	24dd ←→ 24dv
17	BA2 ←→7AL	**34**	Thalamus ←→ cerebellum
Inter-hemispheric connections used in connectome-based analysis			
1	M1 LH ←→ M1 RH	**13**	SCEF LH ←→ 6mp RH
2	M1 LH ←→ 6mp RH	**14**	SCEF LH ←→ SCEF RH
3	M1 LH ←→ 24dd RH	**15**	SCEF LH ←→ 24dd RH
4	M1 LH ←→ thalamus RH	**16**	SCEF LH ←→ 24dv RH
5	6ma LH ←→ 6ma RH	**17**	7Am LH ←→ 7Am RH
6	6ma LH ←→ 6mp RH	**18**	24dd LH ←→ M1 RH
7	6ma LH ←→ SCEF RH	**19**	24dd LH ←→ 6mp RH
8	6mp LH ←→ M1 RH	**20**	24dd LH ←→ SCEF RH
9	6mp LH ←→ 6mp RH	**21**	24dd LH ←→ 24dd RH
10	6mp LH ←→ SCEF RH	**22**	24dv LH ←→ SCEF RH
11	6mp LH ←→ 24dd RH	**23**	Thalamus LH ←→ thalamus RH
12	SCEF LH ←→ 6ma RH	**24**	cerebellum LH ←→ cerebellum RH

3. Results

3.1 Group comparisons

Tables 4 and 5 present the motor area connections that are significantly different from the controls in the LLP and RLP groups. The results of the statistical comparisons are illustrated in Figure 3 for the global motor areas previously defined in Table 2. The Main intra-hemisphere disconnections in the lesioned hemisphere for the LLP group are between M1 and S1, PMC subareas as well as between Thalamus and SMA subareas (see Table 3, Figure 3). This is expected due to the location of the lesions near the M1 and S1 in the left hemisphere for the LLP group (please refer to supplementary Figure A). Then as well, a mirroring disconnection pattern was observed in the contra-lesioned hemisphere (RH) for the LLP group. This was observed as a significantly lower connectivity between M1 and S1. There were also disconnection between S1 and Thalamus (Table 3, Figure 3). Regarding inter-hemisphere connections, no significant disconnections were observed for the LLP compared to the healthy control group.

LLP and Controls group comparison also revealed higher connectivity scores between the thalamus and the S1 (Table 3) in the lesioned hemisphere in addition to increased connection between M1 and SMA of the contra-lesioned hemisphere. But more importantly increase in interhemisphere connections were observed between left and right thalamus and cerebellum and between the left CC and right SMA.

Similar results were depicted for the RLP group as displayed in Table 5. Primary disconnections in the lesioned hemisphere (RH) were found between M1 and PMC as well as between S1 and thalamus (See Table 5, Figure 3). Similarly to the LLP group, the contra-lesioned hemisphere of the RLP patients exhibited a decrease in the connection scores between motor

areas equivalent to the ones observed in the lesioned hemisphere (Table 5, Figure 3). RLP patients also demonstrated higher connections than controls in the lesioned hemisphere between S1 and thalamus and in the contralesioned hemisphere between M1 and cerebellum. Furthermore, interconnections between the left and right thalamus were found to be greater than in the control group.

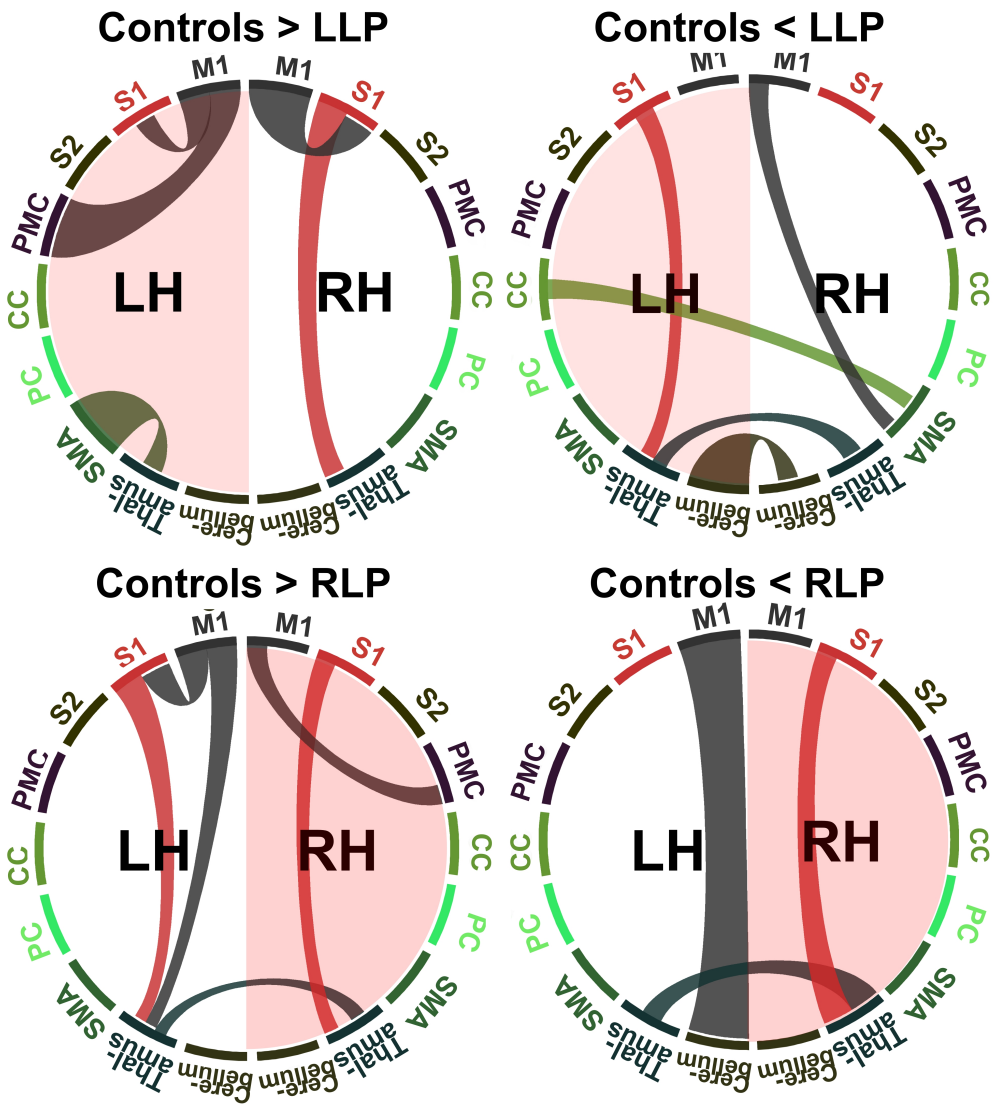

Figure 3: Circular representation of the significantly different structural connectivity tracts between patients (LLP and RLP) and controls for the different motor areas defined in Table 2.

Table 4: The significant difference results of the structural connectivity strength comparison between controls and LLP groups.

	Controls > LLP			Controls < LLP		
	Area	Subsection	p-value	Area	Subsection	p-value
Intra LH (ipsi)	M1 ⇔ S1	M1 ⇔ BA1	0.00706	S1 ⇔ Thalamus	BA2 ⇔ Thalamus	0.0261
	M1 ⇔ PMC	M1 ⇔ 6V	0.0030			
	Thalamus ⇔ SMA	Thalamus ⇔ 6ma	0.0375			
Intra RH (contra)	M1 ⇔ S1	M1 ⇔ BA3a	0.0070	M1 ⇔ SMA	M1 ⇔ 6mp	0.0329
	S1 ⇔ Thalamus	BA1 ⇔ Thalamus	0.0279			
Inter H				LH CC ⇔ RH SMA	LH 24dd ⇔ RH SCEF	0.0129
				LH Cerebellum ⇔ RH Cerebellum	LH Cerebellum ⇔ RH Cerebellum	0.0129
				LH Thalamus ⇔ RH Thalamus	LH Thalamus ⇔ RH Thalamus	0.0178

Table 5: The significant difference results of the structural connectivity metric comparison comparison between controls and RLP groups.

	Controls > RLP			Controls < RLP		
	Area	Subsection	p-value	Area	Subsection	p-value
Intra RH (ipsi)	M1 ⇔ PMC	M1 ⇔ 6V	0.0470	S1 ⇔ Thalamus	BA3a ⇔ Thalamus	0.0317
	S1 ⇔ Thalamus	BA1 ⇔ Thalamus	0.0161			
Intra LH (contra)	M1 ⇔ S1	M1 ⇔ BA1	0.0028	M1 ⇔ Cerebellum	M1 ⇔ Cerebellum	0.0436
	M1 ⇔Thalamus	M1 ⇔ Thalamus	0.0038			
	S1 ⇔ Thalamus	BA3a ⇔Thalamus	0.0047			
		BA1 ⇔ Thalamus	0.0228			
		BA2 ⇔ Thalamus	0.0077			
Inter H				LH Thalamus ⇔ RH Thalamus	LH Thalamus ⇔ RH Thalamus	0.0248

3.2 BBT score correlation analysis and prediction

In order to identify the connections that are correlated to the motor outcome for both LLP and RLP groups we computed the linear correlation between the BBT score and all the motor area connections scores of the corresponding hemisphere. Table 6 displays the intra-hemisphere connections that are linearly correlated to the contralesional and ipsilesional hands BBT scores for the LLP and RLP groups. In the case of LLP group, the contralesional hand BBT score was found to be positively correlated to the ipsilesional connectivity weight between the

thalamus and PC and negatively correlated to the connectivity weight between the CC and thalamus. In addition, a negative correlation was found between the ipsilesional hand BBT score and the contralesional connection weight between the M1 and thalamus and positive correlations between the thalamus and the cerebellum as well as between S1 subareas.

For the RLP group, we found positive correlations between S1 subareas connectivity weights and the contralesional BBT and a negative correlation with the S1 and M1 connections. for the ipsilesional BBT no significant correlations were depicted with the connectivity scores.

Table 6: The motor connection that are linearly correlated to the BBT in the case of the LLP and RLP groups. The most significantly correlated connections to the BBT score are depicted in bold red

		Areas	**Subsections**	**R**	**P-value**
LLP	Contralesional BBT	LH PC ⇔ LH Thalamus	LH 7AL ⇔ LH Thalamus	0.5902	0.0099
		LH CC ⇔ LH Thalamus	LH 24dd ⇔ LH Thalamus	-0.5338	0.0225
	Ipsilesional BBT	RH M1 ⇔ RH Thalamus	RH M1 ⇔ RH Thalamus	-0.6000	0.0085
		RH S1⇔ RH S1	RH BA3a ⇔ RH BA2	0.4825	0.0425
		RH Thalamus ⇔ RH Cerebellum	RH Thalamus ⇔ RH Cerebellum	0.5099	0.0306
RLP	Contralesional BBT	RH M1 ⇔ RH S1	RH M1 ⇔ RH BA3a	-0.5861	0.0276
		RH S1 ⇔ RH S1	RH BA3a ⇔ RH BA2	0.5508	0.0412
	Ipsilesional BBT	___	____	____	_____

The prediction accuracy following the leave-one-participant-out cross validation technique of the BBT score based on the connections of interest identified in Table 6 for each group and each hand is depicted in Table 7. These results highlight a similar prediction BBT score for both groups with a slightly better performance when combining all the connectivity scores compared to only the most significant one.

Table 7: The Accuracy of predicting BBT scores**. The most significant connectivity scores were presented in Table 6 (red)**

	BBT	**Most significant connectivity score**	**All connectivity scores**
LLP	Contralesional	65.50%	70.02%
	Ipsilesional	83.14%	86.52%
RLP	Contralesional	79.90%	81.05%
	Ipsilesional	—-	——

3.2 CP correlation analysis and prediction

Finally, with regard to the presence or not of CP, one connection of interest was identified for each both groups. These connections were between the PMC subareas (the frontal eye field and the anterior part of BA6). The connectivity score associated with these regions exhibited a significantly positive point biserial correlation with the absence of CP. Using these specific connection scores we were able to deliver a good classification accuracy for both groups (please refer to Table 8).

Table 8: The motor connection that are correlated with the CP presence/absence and the results of the classification of patients between CP and non-CP using these connections.

	Connection	Correlation value	p-value	Classification accuracy
LLP	LH PMC (6a) ⇔ LH PMC (FEF)	0.5035	0.0332	94.44%
RLP	RH PMC (6a) ⇔ RH PMC (FEF)	0.5660	0.0310	85.71%

4. Discussion

In this work, we used fiber tractography and high resolution connectomics in order to evaluate the relationship between specific disconnections between motor areas and motor outcome at age 7 following neonatal stroke. One of the main findings is that disconnections observed in the contralesioned hemisphere mimics those found in lesioned hemispheres in both LLP and RLP groups near the lesion area (please refer to supplementary figure A). This shows that even though there is no lesion (by definition) in the contralesioned ("healthy") hemisphere, still it suffers from the neonatal stroke consequences, with a decreased connectivity between regions similar to those found in the lesioned hemisphere compared to healthy controls. These regions are mainly within and between S1 and M1 (close to the lesion site) as well as between S1, M1 and thalamus, PMC respectively. This can be seen as a direct result of the stroke infarct where the disconnections in the thalamus are reflected in a decreased connectivity through the feed forward processing function (Eccles, 2013).

Another important finding in the present study is that higher connectivity weights were found in patients groups compared to healthy controls. This higher connectivity was observed more often in inter-hemispheric than in intra-hemispheric connections, where it was observed only

, in a few nodes, i.e. between the ipsilesional thalamus and S1 for both groups and between the contralesional M1 and cerebellum/SMA (RLP/LLP). In the case inter-hemispheric connections, stronger connections were observed between the left and right thalamus for both groups and between left and right cerebellum for the LLP group. This increased intra-hemispheric connectivity in particular regions in both groups, even though not exactly the same, could portray a compensatory phenomenon in the lesioned hemisphere wherein the thalamus plays a major role in motor plasticity and is as a major hub for motor system. It has been demonstrated that remaining neurons in the peri-infarct cortex go through a structural remodeling that is linked with a remapping of lost functions (Silasi and Murphy, 2014). Therefore, it is conceivable that the increase in the aforementioned connectivity can be a form of (re)organization phenomenon.

Moreover, in the LLP group, an increase in the inter-hemisphere connections was observed between the contralesional SMA and the ipsiesional CC (please refer to Table 4).This can be seen as a compensatory mechanism to the disconnections mentioned earlier. However, this is only speculative. Giving other explanation on why we found increase connectivity in some particular regions (regions depending on the side of the infarct) in our patients is not a trivial task.

Correlation analysis between the BBT score and the connectivity score revealed valuable input about the motor outcome following NAIS. We found a significant positive correlation between the contralesional hand motor score and ipsilesional connections in the LLP group (Tables 4 and 6). These fibers connect the thalamus and the PC, indicating that a higher score is directly linked to the amount of compensatory fibers between the thalamus and PC following the stroke. Concerning the negative correlation found between the contralesional BBT score

and the ipsilesional intra-hemispheric connectivity between the CC and the thalamus connection weight, it can demonstrate the role of these regions in motor inhibitory system (Dinomais et al., 2009; Mangia et al., 2017; Wardak, 2011), which is dominant in the right hemisphere (Verfaellie and Heilman, 1987). In other terms, our results support the fact that higher connectivity in region playing a role in inhibitory system, could be accompanied by poorer motor performance. For the ipsilesional BBT score the positive correlations were for the connections between the thalamus and cerebellum as well as between the subareas of S1 in the contralesioned hemisphere. The negative correlations were found between M1 and the thalamus. The importance of the thalamus in predicting hand motor function has been already discussed many times (Holmefur et al., 2013; Ryll et al., 2019). These results indicates that the thalamus connections with other motor regions is directly linked to motor score as it was demonstrated recently by (Craig et al., 2019).

In the RLP group, correlation analysis showed a linear positive correlation between the contralateral hand BBT score and the ipsilesional intra-hemispheric connectivity weight between M1 and S1 which were found lower than in the control group. For the ipsilesional hand BBT score we did not find significant correlations with the connectivity scores. This can be explained by the low standard deviation between ipsilesional and contralesional BBT scores for the RLP groups as well as the low number of patients. Using the connections of interest, we were able to estimate the BBT score with good enough accuracy.

Finally, we computed the point biserial correlation between the connectivity weight and the CP presence/absence. We only found one connection of interest for both group of patients. This connection concerned the PMC confirming its central role in motricity following a brain lesion. Based solely on this connection weight, we were able to classified the patients with

regard to the presence/absence of CP with good accuracy. This highlights the direct link between the weight of these structural connections and the presence of CP. Our results confirm that the preservation or not of connections in the PMC can be a predictor of the presence or absence of CP after unilateral early brain lesion. This is consistent with studies that showed that primary motor cortices are altered in children with CP (Kurz et al., 2017).

To conclude this discussion, we have to mention some of the limitations of this work. The main limitation of this study was the absence of the BBT score for the control group which would have provided an extra layer for our correlation analysis and validated our results. Another limitation would be the limited sample number for the patients especially after dividing them into two unequal groups (LLP and RLP), however our cohort are very homogenous in terms of age at the evaluation and type of lesion (neonatal stroke is "presented as the ideal human model of developmental neuroplasticity" (Kiton, 2013)). Lastly, we have to note that every neuroimaging method has its limitations and tractography is no exception especially in the lesioned brain. New fixel-based analysis techniques can help to better process the lesioned brain. Future work will include whole brain fixel based analysis of the NAIS brain in order to confirm the results introduced in this article.

5. Conclusions

The present study underlines the importance of tracts inspection in addition to other techniques (lesion mapping, morphometry analysis…) in predicting motor outcome and "recovery" following neonatal stroke. We demonstrated that cortical regions in the ipsilesional as well as contralesional hemispheres exhibit a reduction in connectivity when compared to healthy controls suggesting that cortical areas directly unaffected by the stroke still exhibit fiber losses. Neonatal stroke does not appear to be only a focal lesion but a lesion that impacts

the whole developing brain. We also found an increase in connections portraying some sort of compensatory mechanism in motor areas that could be explained by a structural (re)organization scheme. Finally, we were able to predict motor outcome assessed by BBT scores and CP presence based on connections weights that were linearly correlated to them. We highlighted the importance of the preservation of the connectivity to and from the thalamus. Future work could include a combination of structural analysis with functional connectivity analyses during resting state, which could add further insight into the neonatal stroke impact of different outcomes.

6. Funding

The research was supported by the University hospital of Angers (eudract number 2010-A00976-33), the Ministère de la solidarité et de la santé (eudract number 2010-A00329-30), and the Fondation de l'Avenir (ET0-571). M Al Harrach, was supported by grants obtained from the Fondation pour la Recherche Médicale (FRM-DIC20161236453). Sponsors of the study had no role in the study design data collection, data analysis, data interpretation, writing of the report, or decision to submit for publication.

7. Acknowledgments

8. Conflict of Interest

None declared.

9. References

Andersson, J.L.R., Sotiropoulos, S.N., 2016. An integrated approach to correction for off-resonance effects and subject movement in diffusion MR imaging. NeuroImage 125, 1063–1078. https://doi.org/10.1016/j.neuroimage.2015.10.019

Bioulac, B., Burbaud, P., Cazalets, J.-R., Gross, C., 2004. Fonctions motrices. EMC - Neurologie 1, 277–329. https://doi.org/10.1016/j.emcn.2004.02.002

Bonilha Leonardo, Rorden Chris, Fridriksson Julius, 2014. Assessing the Clinical Effect of Residual Cortical Disconnection After Ischemic Strokes. Stroke 45, 988–993. https://doi.org/10.1161/STROKEAHA.113.004137

Cans, C., Dolk, H., Platt, M., Colver, A., Prasausk1ene, A., Rägeloh−Mann, I.K., 2007. Recommendations from the SCPE collaborative group for defining and classifying cerebral palsy. Developmental Medicine & Child Neurology 49, 35–38. https://doi.org/10.1111/j.1469-8749.2007.tb12626.x

Chabrier, S., Peyric, E., Drutel, L., Deron, J., Kossorotoff, M., Dinomais, M., Lazaro, L., Lefranc, J., Thébault, G., Dray, G., Fluss, J., Renaud, C., Nguyen The Tich, S., 2016. Multimodal Outcome at 7 Years of Age after Neonatal Arterial Ischemic Stroke. The Journal of Pediatrics 172, 156-161.e3. https://doi.org/10.1016/j.jpeds.2016.01.069

Craig BT, Carlson HL, Kirton A. Thalamic diaschisis following perinatal stroke is associated with clinical disability. *Neuroimage Clin*. 2019;21:101660. doi:10.1016/j.nicl.2019.101660

Dinomais, M., Hertz-Pannier, L., Groeschel, S., Chabrier, S., Delion, M., Husson, B., Kossorotoff, M., Renaud, C., Nguyen The Tich, S., for the AVCnn Study Group, 2015. Long term motor function after neonatal stroke: Lesion localization above all. Hum. Brain Mapp. 36, 4793–4807. https://doi.org/10.1002/hbm.22950

Dunbar, M., Kirton, A., 2018. Perinatal stroke: mechanisms, management, and outcomes of early cerebrovascular brain injury. The Lancet Child & Adolescent Health 2, 666–676. https://doi.org/10.1016/S2352-4642(18)30173-1

Feng, W., Wang, J., Chhatbar, P.Y., Doughty, C., Landsittel, D., Lioutas, V.-A., Kautz, S.A.,

Schlaug, G., 2015. Corticospinal tract lesion load: An imaging biomarker for stroke motor outcomes. Annals of Neurology 78, 860–870. https://doi.org/10.1002/ana.24510

Fluss, J., Dinomais, M., Chabrier, S., 2019. Perinatal stroke syndromes: Similarities and diversities in aetiology, outcome and management. European Journal of Paediatric Neurology 23, 368–383. https://doi.org/10.1016/j.ejpn.2019.02.013

Glasser, M.F., Coalson, T.S., Robinson, E.C., Hacker, C.D., Harwell, J., Yacoub, E., Ugurbil, K., Andersson, J., Beckmann, C.F., Jenkinson, M., Smith, S.M., Essen, D.C.V., 2016. A multi-modal parcellation of human cerebral cortex. Nature 536, 171–178. https://doi.org/10.1038/nature18933

Harrach, M.A., Rousseau, F., Groeschel, S., Wang, X., Hertz−pannier, L., Chabrier, S., Bohi, A., Lefevre, J., Dinomais, M., 2019. Alterations in Cortical Morphology after Neonatal Stroke: Compensation in the Contralesional Hemisphere? Developmental Neurobiology 79, 303–316. https://doi.org/10.1002/dneu.22679

Jang, S.H., 2010. Prediction of motor outcome for hemiparetic stroke patients using diffusion tensor imaging: A review. NeuroRehabilitation 27, 367–372. https://doi.org/10.3233/NRE-2010-0621

Kellner, E., Dhital, B., Kiselev, V.G., Reisert, M., 2016. Gibbs-ringing artifact removal based on local subvoxel-shifts. Magnetic Resonance in Medicine 76, 1574–1581. https://doi.org/10.1002/mrm.26054

Kirton, A., deVeber, G., 2015. Paediatric stroke: pressing issues and promising directions. The Lancet Neurology 14, 92–102. https://doi.org/10.1016/S1474-4422(14)70227-3

Kirton, A., DeVeber, G., Pontigon, A.-M., Macgregor, D., Shroff, M., 2008. Presumed perinatal ischemic stroke: Vascular classification predicts outcomes. Annals of Neurology 63, 436–443. https://doi.org/10.1002/ana.21334

Kirton Adam, deVeber Gabrielle, 2013. Life After Perinatal Stroke. Stroke 44, 3265–3271. https://doi.org/10.1161/STROKEAHA.113.000739

Kurz MJ, Proskovec AL, Gehringer JE, Heinrichs-Graham E, Wilson TW. Children with cerebral palsy have altered oscillatory activity in the motor and visual cortices during a knee motor task. *Neuroimage Clin*. 2017;15:298-305. Published 2017 May 15. doi: 10.1016/j.nicl.2017.05.008

Lam, T.K., Binns, M.A., Honjo, K., Dawson, D.R., Ross, B., Stuss, D.T., Black, S.E., Chen, J.J., Fujioka, T., Chen, J.L., 2018. Variability in stroke motor outcome is explained by structural and functional integrity of the motor system. Sci Rep 8, 1–11. https://doi.org/10.1038/s41598-018-27541-8

Lim, S., Han, C.E., Uhlhaas, P.J., Kaiser, M., 2015. Preferential Detachment During Human Brain Development: Age- and Sex-Specific Structural Connectivity in Diffusion Tensor Imaging (DTI) Data. Cereb Cortex 25, 1477–1489. https://doi.org/10.1093/cercor/bht333

Lin, L.Y., Ramsey, L., Metcalf, N.V., Rengachary, J., Shulman, G.L., Shimony, J.S., Corbetta, M., 2018. Stronger prediction of motor recovery and outcome post-stroke by cortico-spinal tract integrity than functional connectivity. PLoS One 13. https://doi.org/10.1371/journal.pone.0202504

Mathiowetz, V., Volland, G., Kashman, N., Weber, K., 1985. Adult Norms for the Box and Block Test of Manual Dexterity. Am J Occup Ther 39, 386–391. https://doi.org/10.5014/ajot.39.6.386

Oldfield, R.C., 1971. The assessment and analysis of handedness: The Edinburgh inventory. Neuropsychologia 9, 97–113. https://doi.org/10.1016/0028-3932(71)90067-4

Raffelt, D.; Dhollander, T.; Tournier, J.-D.; Tabbara, R.; Smith, R. E.; Pierre, E. & Connelly, A. Bias Field Correction and Intensity Normalisation for Quantitative Analysis of Ap-

parent Fibre Density. In Proc. ISMRM, 2017, 26, 3541

Rorden, C., Karnath, H.-O., Bonilha, L., 2007. Improving Lesion-Symptom Mapping. Journal of Cognitive Neuroscience 19, 1081–1088. https://doi.org/10.1162/jocn.2007.19.7.1081

Rowe, J.B., Siebner, H.R., 2012. The motor system and its disorders. NeuroImage, NEUROIMAGING: THEN, NOW AND THE FUTURE 61, 464–477. https://doi.org/10.1016/j.neuroimage.2011.12.042

Smith, R.E., Tournier, J.-D., Calamante, F., Connelly. A. SIFT: Spherical-deconvolution informed filtering of tractograms. NeuroImage 67 (2013), pp. 298–312.

Song, J., Nair, V.A., Young, B.M., Walton, L.M., Nigogosyan, Z., Remsik, A., Tyler, M.E., Farrar-Edwards, D., Caldera, K.E., Sattin, J.A., Williams, J.C., Prabhakaran, V., 2015. DTI measures track and predict motor function outcomes in stroke rehabilitation utilizing BCI technology. Front. Hum. Neurosci. 9. https://doi.org/10.3389/fnhum.2015.00195

Taylor, P.N., Sinha, N., Wang, Y., Vos, S.B., de Tisi, J., Miserocchi, A., McEvoy, A.W., Winston, G.P., Duncan, J.S., 2018. The impact of epilepsy surgery on the structural connectome and its relation to outcome. NeuroImage: Clinical 18, 202–214. https://doi.org/10.1016/j.nicl.2018.01.028

Taylor, P.N., Wang, Y., Kaiser, M., 2017. Within brain area tractography suggests local modularity using high resolution connectomics. Sci Rep 7, 1–9. https://doi.org/10.1038/srep39859

Tournier, J.-D., Calamante, F., Connelly, A., 2009. Improved probabilistic streamlines tractography by 2 nd order integration over fibre orientation distributions.

Tournier, J.-D., Calamante, F., Connelly, A., 2007. Robust determination of the fibre orientation distribution in diffusion MRI: Non-negativity constrained super-resolved spherical deconvolution. NeuroImage 35, 1459–1472. https://doi.org/10.1016/j.neuroimage.

2007.02.016

Tournier, J.-D., Calamante, F., Gadian, D.G., Connelly, A., 2004. Direct estimation of the fiber orientation density function from diffusion-weighted MRI data using spherical deconvolution. NeuroImage 23, 1176–1185. https://doi.org/10.1016/j.neuroimage.2004.07.037

Veraart, J., Fieremans, E., Novikov, D.S., 2016a. Diffusion MRI noise mapping using random matrix theory. Magnetic Resonance in Medicine 76, 1582–1593. https://doi.org/10.1002/mrm.26059

Veraart, J., Novikov, D.S., Christiaens, D., Ades-aron, B., Sijbers, J., Fieremans, E., 2016b. Denoising of diffusion MRI using random matrix theory. NeuroImage 142, 394–406. https://doi.org/10.1016/j.neuroimage.2016.08.016

Xie, T., He, Y., 2012. Mapping the Alzheimer's Brain with Connectomics. Front. Psychiatry 2. https://doi.org/10.3389/fpsyt.2011.00077

Yoo, Y.J., Kim, J.W., Kim, J.S., Hong, B.Y., Lee, K.B., Lim, S.H., 2019. Corticospinal Tract Integrity and Long-Term Hand Function Prognosis in Patients With Stroke. Front. Neurol. 10. https://doi.org/10.3389/fneur.2019.00374

Yourganov, G., Fridriksson, J., Rorden, C., Gleichgerrcht, E., Bonilha, L., 2016. Multivariate Connectome-Based Symptom Mapping in Post-Stroke Patients: Networks Supporting Language and Speech. J. Neurosci. 36, 6668–6679. https://doi.org/10.1523/JNEUROSCI.4396-15.2016

.